Biosensors and Bioelectronics 58 (2014) 179–185

Contents lists available at ScienceDirect

Biosensors and Bioelectronics

journal homepage: www.elsevier.com/locate/bios

A nanoceria–platinum–graphene nanocomposite for electrochemical biosensing

P. Chaturvedi [a,1], D.C. Vanegas [a,b,1], M. Taguchi [a], S.L. Burrs [a], P. Sharma [c], E.S. McLamore [a,*]

[a] Agricultural & Biological Engineering, University of Florida, USA
[b] Food Engineering, Universidad del Valle, Colombia
[c] Material Science & Engineering, University of Florida, USA

ARTICLE INFO

Article history:
Received 31 October 2013
Received in revised form
25 January 2014
Accepted 10 February 2014
Available online 26 February 2014

Keywords:
Glucose oxidase
Xanthine oxidase
Nanoceria
Graphene
Amperometry

ABSTRACT

Most graphene–metal nanocomposites for biosensing are formed using noble metals. Recently, development of nanocomposites using rare earth metals has gained much attention. This paper reports on the development of a nanoceria–nanoplatinum–graphene hybrid nanocomposite as a base transducing layer for mediator-free enzymatic biosensors. The hybrid nanocomposite was shown to improve detection of superoxide or hydrogen peroxide when compared to other carbon–metal hybrid nanocomposites. Based on this finding, the nanocomposite was applied for biosensing by adding either a peroxide-producing oxidase (glucose oxidase), or a superoxide-producing oxidase (xanthine oxidase). Material analysis indicated that nanoceria and nanoplatinum were equally distributed along the surface of the hybrid material, ensuring detection of either superoxide or hydrogen peroxide produced by oxidase activity. Glucose biosensors demonstrated a sensitivity (66.2 ± 2.6 μA mM^{-1} cm^{-2}), response time (6.3 ± 3.4 s), and limit of detection (1.3 ± 0.6 μM) that were comparable to other graphene–mediated electrodes in the current literature. Remarkably, XOD biosensor sensitivity (1164 ± 332 μA mM^{-1}), response time (5.0 ± 1.5 s), and limit of detection (0.2 ± 0.1 μM) were higher than any reported biosensors using similar metal-decorated carbon nanomaterials. This material is the first demonstration of a highly efficient, diverse nanoceria/nanoplatinum/graphene hybrid nanocomposite for biosensing.

1. Introduction

Rare earth metal oxides such as cerium oxide (CeO_2) have been used for decades as catalysts in devices such as solar cells, fuel cells, automobile catalytic converters, and oxygen storage systems (Adachi and Imanaka, 1997; F. Zhang et al., 2010a, 2010b; Lu et al., 2011). The catalytic activity of CeO_2 is due to fast transition between Ce(III) and Ce(IV), changing the oxygen vacancies and forming *n*-type hybrids (Joung et al., 2011). Various forms of nanoscale CeO_2 (known as nanoceria) have recently been shown to significantly improve electro and photocatalysis (Nyk et al., 2008; Neil et al., 2011). Zhou et al. (2005) developed CeO_2 nanorods for enhanced carbon monoxide (CO) conversion efficiency with applications in catalytic converters (Joung, et al., 2011; Jiang et al., 2012; Ji et al., 2013). Gaynor et al. (2013) developed a spectrophotometric device for enzyme-free detection of hydrogen peroxide (H_2O_2) using oxygen deficient nanoceria.

Graphene, composed of a monolayer of carbon atoms in a honeycomb allotrope, has received much attention in recent years due to its excellent mobility of charge carriers, high specific surface area, and superb electrical/thermal conduction (Bolotin et al., 2008; Geim and Novoselov, 2007; Geim, 2009; Li et al., 2008; Rao et al., 2009; Stankovich et al., 2006). Reduction of water soluble graphene oxide (GO) to reduced graphene oxide (RGO) produces a highly conductive material due to oxygen vacancies along the surface of allotropic sheets (Zhu et al., 2010). GO has been reduced using chemical agents such as hydrazine (Stankovich et al., 2007), hydroquinone (Wang et al., 2008), sodium borohydride (Sun et al., 2013), and ascorbic acid (Dua et al., 2010). Thermal treatment (Schniepp et al., 2006) and solar exfoliation (Aravind et al., 2011) have also been used to reduce GO.

Composites of graphene with various metal oxides have been developed for use in devices such as fuel cells, sensors, batteries, and solar cells (Akhavan, 2011; Bai and Shen, 2012; Du et al., 2011; Liang et al., 2011; Luo et al., 2012; Wang et al., 2009; Wu et al., 2010a; Yang et al., 2011; Zhang et al., 2010). Graphene–metal nanocomposites have unique properties that are significantly improved over the bulk metal and metal oxide alone (Liang et al., 2011; Wu et al., 2010a, 2010b; Kim et al., 2009; Stankovich et al., 2006; Li et al., 2012; Huang et al., 2012). This effect is due to

* Corresponding author.
E-mail address: emclamor@ufl.edu (E.S. McLamore).
[1] Authors contributed equally to this work.

http://dx.doi.org/10.1016/j.bios.2014.02.021
0956-5663

the ability of metal oxides to maintain the interplanar spacing of the graphene sheets, preventing aggregation into graphitic structures and improving electron transport (Huang et al., 2011).

In the last 3 years, a number of researchers have created nanoceria–graphene nanocomposites that could be useful in biosensing. Jiang et al. (2013) demonstrated tunable synthesis of ceria nanocrystal/graphene hybrid nanostructures (including nanorods, nanoparticles, and nanocubes). The material demonstrated excellent photocatalytic and electrocatalytic effects. Wang et al. (2011) demonstrated use of nanoceria–graphene composites for high efficiency batteries; the material showed extremely high specific capacitance, power density, and behaved as a super capacitor. Jiang et al. (2012) synthesized crystalline CeO_2 nanocubes hybridized with graphene sheets using a hydrothermal method. The nanocomposites were immobilized on a glassy carbon electrode and used to detect uric acid and ascorbic acid. Wang et al. (2011) synthesized CeO_2–graphene nanocomposites using stimuli-responsive polymers. The only report of nanoceria hybrid composites used together with immobilized proteins was Asati et al. (2009); nanoceria-based immunoassays were developed for catalysis of organic dyes such as tetramethyl benzidin. While each of these materials is promising for biosensing applications, validation studies are needed to confirm the catalytic behavior of nanoceria–graphene composites are conserved once proteins are immobilized on the surface.

This paper demonstrates use of nanoceria–graphene–nanoplatinum hybrid nanocomposite as a platform for developing electrochemical biosensors based on oxidase enzymes (Fig. 1). The simple recipe can be reproduced at room temperature using common/inexpensive materials, and produces a transducer platform for fabrication of high quality biosensors with excellent electroactive surface area, sensitivity, response time, and limit of detection. The platform is demonstrated for development of glucose and xanthine biosensors.

2. Methods

2.1. Materials and reagents

Graphene oxide was obtained from ACS Material; L-ascorbic acid and methanol were purchased from Fisher Scientific; cerium (IV) oxide (nanoparticles dispersion, <25 nm particle size, 10 wt% in H_2O), chloroplatinic acid 8 wt%, glucose oxidase (GOx), and xanthine oxidase (XOD) were procured from Sigma-Aldrich; D(+); glucose, xanthine (98%), hydrogen peroxide (35%), tetraethyl orthosilicate (98% TEOS), hydrochloric acid (37% HCl), and potassium nitrate (KNO_3) were acquired from Acros organics; potassium ferrocyanide trihydrate ($K_4Fe(CN)_6$) was purchased from EMD chemicals; laponite RD was obtained from Southern Clay Products; PBS, and TRIZMA buffers were procured from Mediatech, Inc.

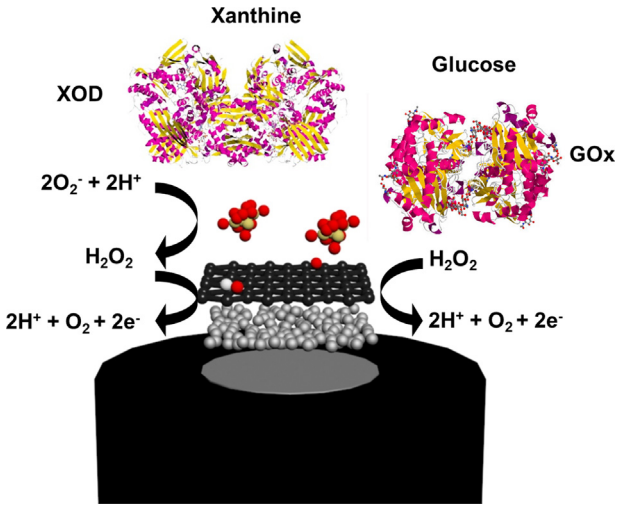

Fig. 1. The hybrid nanocomposite catalyzes detection of superoxide (nanoceria) or hydrogen peroxide (graphene–platinum). In this paper, oxidase enzymes that produce either superoxide (xanthine oxidase) or hydrogen peroxide (glucose oxidase) as a byproduct are demonstrated.

2.2. Nanomaterial deposition

Prior to analysis, Pt/Ir working electrodes (BASI MF-2013, 1.6 mm diameter, 7.5 cm length, 6 mm shaft diameter, CTFE plastic body) were polished with 3 μm, and 1 μm polycrystalline diamond suspensions (Buehler®, USA). Electrodes were then rinsed with methanol, and polished with 0.05 μm alumina slurry (Buehler®, USA). After polishing, all electrodes were ultrasonicated in deionized water for 15 min.

Amorphous nanoplatinum clusters (nPt) were formed on the surface of the electrode via sonoelectrodeposition at 10 V for 30 s in a solution of 1.44% chloroplatinic acid and 0.002% lead acetate according to our previously published methods (McLamore et al., 2011; Shi et al., 2011; Vanegas et al., 2014). A graphene/nanoceria suspension was prepared by mixing 1 mL of cerium (IV) oxide nanoparticle suspension (mean nanoparticle size=12 nm) with 2 mg of single-layer graphene oxide (SLGO) powder and 8 mg of L-ascorbic acid. The suspension was ultrasonicated for 30 min. Immediately after sonication, a 2 μL aliquot of the nanoparticle suspension was spin-coated at 2600 rpm on nPt-modified electrodes, air-dried, and then rinsed. Finally, another layer of nPt was electrodeposited on the nCe–RGO composite by sonoelectrodeposition (42 kHz) at 10 V for 30 s.

2.3. Enzyme immobilization

Laponite hydrogel (1%) was prepared in TRIZMA buffer and ultrasonicated for 2 h. Sol–gel was prepared by mixing 5 g of TEOS with 4.33 g of deionized water and 2.3 g of HCl (0.04 M); sol–gel was vortex-agitated for 1 h. Approximately 10 mg of enzyme (GOx or XOD) was mixed with 20 μL of laponite hydrogel. An aliquot (2 μL) of the resulting hydrogel was spin coated on the surface of nanomaterial modified electrodes at 2600 rpm for 10 min. Finally, the tip of the electrode was immersed in sol–gel for 10 min and then air dried for 5 min. The final sol–gel layer was included to reduce leaching of enzymes from the hydrogel layer.

2.4. Electrochemical analysis

Electrochemical characterization was performed using a 3 electrode cell stand (C-3, BASi, West Lafayette, IN). Cyclic voltammetry was carried out in 4 mM $Fe(CN)_6$/1 M KNO_3 solutions at a switching potential of 600 mV, versus a Ag/AgCl reference electrode with 5 s quiet time, and scan rates of 20, 50, 100, 125, 150, and 200 mV/s. The electroactive surface area of the nanomaterial mediated electrodes was determined using the Randles–Sevcik equation (scheme 1):

$$i_p = (2.69 \times 10^5) n^{3/2} D^{1/2} C A \nu^{1/2} \quad \text{(scheme1)}$$

where i_p is the redox peak obtained from the cyclic voltammogram, n is the number of transferred electrons in the redox reaction, D is the diffusion coefficient, C is the molar concentration of the working solution, A is the electroactive surface area of the electrode and ν is the potential scan rate.

DC potential amperometry (DCPA) was conducted in PBS at a working potential of +300 mV versus a Ag/AgCl reference electrode with a sampling rate of 1 kHz. The working solution was polarized for 1 h; the current output was measured at constant

potential while successively injecting analyte (H_2O_2, glucose, or xanthine) in the stirred solution (450 rpm) at 2 min intervals until the electrical signal reached steady state (less than 5% deviation).

2.5. Material analysis and imaging

SEM micrographs were taken on a FEI XL-40 FEG-SEM, with accelerating voltage of 30 kV, working distance of 10–11 mm and spot size 3–4 nm. Prior to SEM and EDX analysis, all samples were sputtered with a gold–palladium alloy to form a thin conductive coating on the sample surface (2–5 nm thick). EDS spectra were collected with the EDAX TEAMTM software suite, using a FEI XL-40 FEG-SEM, with accelerating voltage of 30 kV, Magnification of 1000 ×, and resolution of 132 eV.

3. Results and discussion

3.1. Electrochemical performance of hybrid nanocomposite toward H_2O_2

To conduct a baseline comparison for biosensors developed with oxidase enzymes, electroactive surface area in 4 mM $K_4Fe(CN)_6$, and sensitivity towards H_2O_2 were first measured for various arrangements of nCe, nPt, and RGO. Representative cyclic voltammograms and DCPA time series during hydrogen peroxide injection are shown in Fig. 2 (see Fig. S1 for additional data). The electroactive surface area of bare, unmodified Pt/Ir electrodes was $1.9 \pm 0.2 \times 10^{-2}$ cm^2 (Fig. 3b). Deposition of nPt onto bare Pt/Ir electrodes increased surface area by 53% ($2.9 \pm 0.1 \times 10^{-2}$ cm^2). When RGO was spin coated on nPt-modified electrodes, electroactive surface area increased by approximately 168% ($5.1 \pm 0.2 \times 10^{-2}$ cm^2). The electrocatalytic behavior of the RGO hybrid nanocomposites is due to transformation of GO to reduced *n*-type hybrids (Joung et al., 2011), and formation of junctions between RGO and the nPt-modified electrode. Similar effects have been observed in other metal–graphene composites, where metal oxides uniformly dispersed on the plane of graphene facilitated charge transfer (Jiang et al., 2012; Ji et al., 2013; Vanegas et al., 2014). Conversely, deposition of nCe onto bare Pt/Ir reduced electroactive surface area by approximately 21% ($1.5 \pm 2.0 \times 10^{-2}$ cm^2). This result was surprising, as Ansari et al., (2008) and Solanki et al. (2009) showed that nanostuctured cerium oxide (35 nm) was an electrocatalyst. This discrepancy is likely due to the indium-tin-oxide (ITO) that was included in the design by Solanki et al. (2009). The manuscript did not investigate whether the nCe, ITO, or nCe–ITO interaction was the source of the catalysis. For our work, when the RGO–nCe suspension was spin coated on the nPt-modified electrode, electroactive surface area was increased by 63% ($3.1 \pm 1.6 \times 10^{-2}$ cm^2), however it was not higher than a nPt–RGO modified electrode. The highest electroactive surface area (6.2×10^{-2} cm^2) was observed for

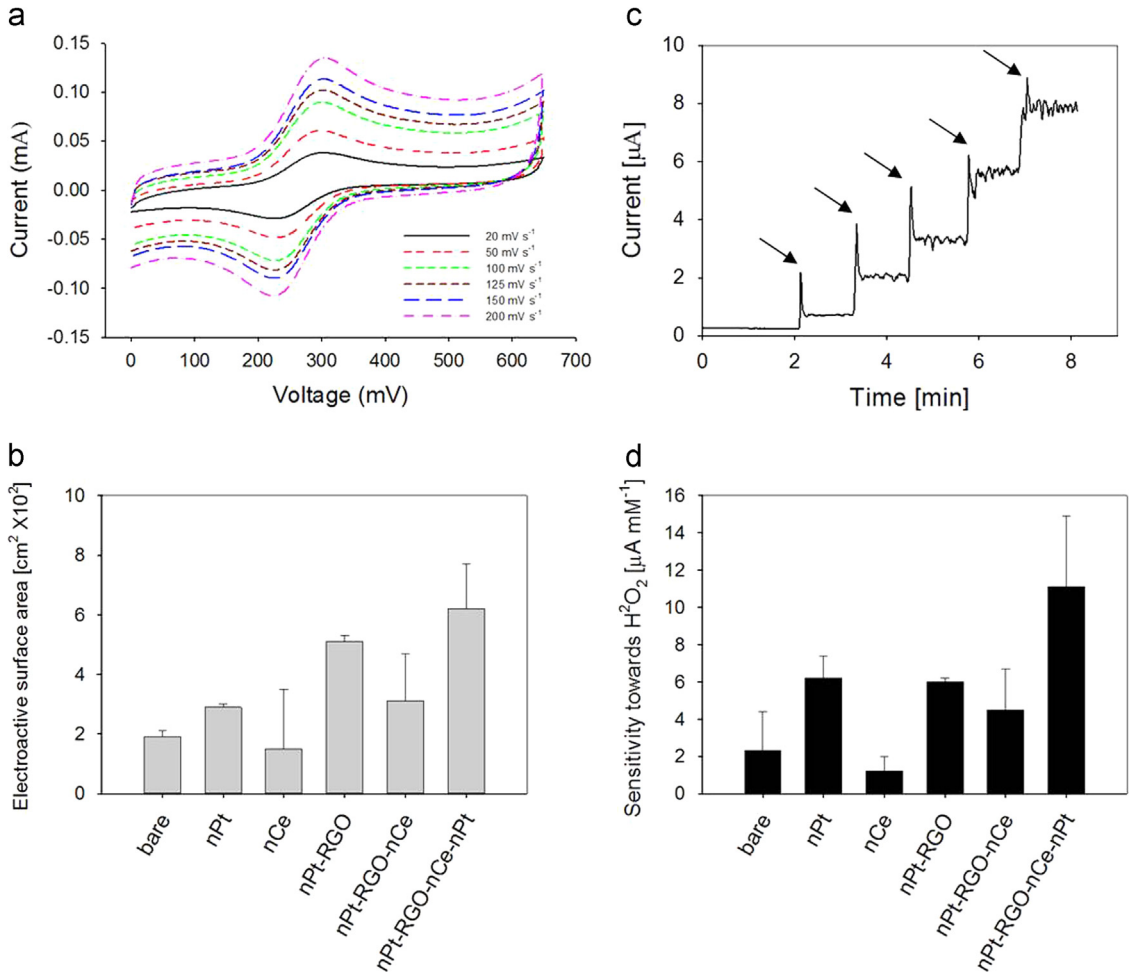

Fig. 2. Electrochemical performance of metal–graphene hybrid nanocomposites. (a) Representative cyclic voltammograms in 4 mM FeKCN for Pt/Ir electrode modified with nPt-RGO-nCe-nPt hybrid nanocomposite at various scan rates. (b) Average electroactive surface area of hybrid nanocomposites formed with nanoceria, nanoplatinum and reduced graphene oxide. (c) Representative sensitivity of nPt-RGO-nCe-nPt electrodes towards H_2O_2. (d) Average sensitivity toward H_2O_2 for hybrid nanocomposites formed with nanoceria, nanoplatinum and reduced graphene oxide (arrows indicate addition of H_2O_2).

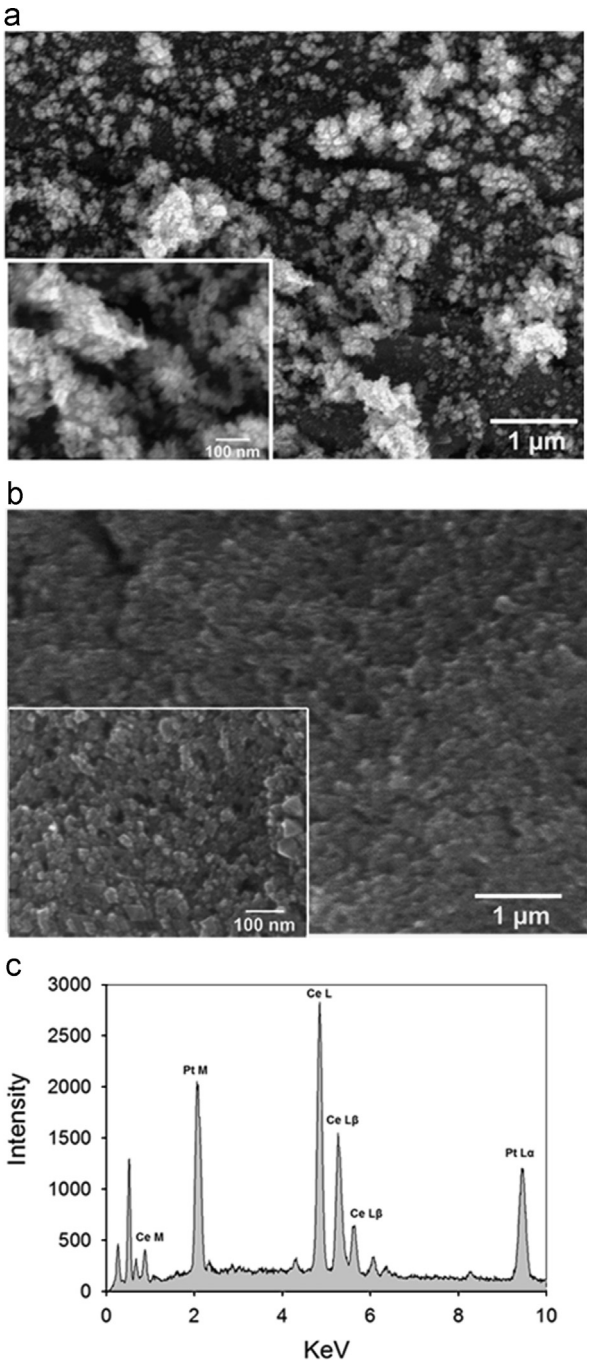

Fig. 3. Material characterization of graphene–metal hybrid nanocomposites. (a) Representative SEM of nPt–RGO–nCe nanocomposite. Nanoceria formed 20 nm aggregates (inset shows exploded view of image in panel a) (b) SEM image of nPt-RGO-nCe-nPt nanocomposite. A homogenous nPt–nCe layer on the surface enhances electroactive surface area (c) EDX spectra confirm the presence of both cerium and platinum in the upper layers of the nanocomposite.

hybrid nPt–RGO–nCe nanocomposites with a second deposition of nPt on top of the nCe (i.e., nPt–RGO–nCe), which is similar to the "sandwich" structure developed by Vanegas et al. (2014). This increase in electroactive surface area is due to the availability of Pt sites along the surface of nCe-modified graphene (see Fig. 3c and related discussion).

A representative DCPA plot showing sensitivity of the nPt–RGO–nCe composite hybrid nanomaterial toward H_2O_2 is shown in Fig. 2c. When comparing the various hybrid nanocomposites previously discussed, similar trends were noted regarding the inclusion of nPt, RGO, and nCe. Composites of nPt and RGO had a high sensitivity toward H_2O_2 ($\approx$160% higher than bare Pt/Ir). Electrodes with nCe as the upper most layer had a relatively low sensitivity toward H_2O_2 (a loss of $\approx$48% sensitivity). The highest sensitivity toward H_2O_2 was for the nanocomposite which contained nPt–RGO–nCe-nPt ($11.1 \pm 3.8\ \mu A\ mM^{-1}$), which is nearly a four-fold increase in sensitivity compared to bare Pt/Ir and a two fold increase over RGO–nCe. The data in Fig. 2 support the conclusion by Huang et al. (2011) that graphene–metal nanocomposites have ordered interplanar spacing that prevents aggregation into graphitic structures and maintains high electron transport efficiency. Our results indicate that nPt is more efficient than nCe for maintaining high electron mobility in RGO. The lower limit of detection (LOD) for the nPt–RGO–nCe-nPt hybrid was 2.6 μM, and the response time was $\approx$3 s. A selectivity analysis was performed according to Shi et al. (2011) to test interference by electroactive species such as ascorbic acid (AA) and uric acid (UA). In the absence of Nafion, addition of AA or UA caused an average interference of $+85 \pm 12\%$. When a Nafion layer was added as the outermost component of the hybrid bio-nanocomposite, addition of AA and UA produced a change in signal which was less than 1% ($+1.2 \pm 1.3\%$, and $+1.9 \pm 1.4\%$). As discussed by Wu et al. (2007), the combination of low operating potential and inclusion of Nafion significantly improve selectivity over UA and AA. Fig S2 shows a representative plot of the selectivity towards H_2O_2 with and without a Nafion layer.

Fig. 3 shows a representative SEM of as-prepared nPt–RGO–nCe (Fig. 3a) and nPt–RGO–nCe-nPt (Fig. 3b) hybrid composites. In Fig. 3a, agglomerates of nanoceria are clearly visible.These structures are similar to the morphology reported by Sun et al. (2013) and Panky et al. (2013). When nCe aggregates were electroplated with nPt, the surface was more homogeneous and contained nPt spheres approximately 20 nm in diameter. The size of these nanospheres is similar to nPt structures deposited on carbon nanotubes (Claussen et al., 2011; McLamore et al., 2011). EDS analysis (panel c) indicated that the nPt structures (two different types of Pt) were intercalated with nCe (four different types of Ce). In fact, the relative elemental composition of the upper layer was balanced with Pt and Ce, containing $53.1 \pm 3.8\%$ platinum and $47.9 \pm 3.3\%$ cerium. The trend for most graphene–metal composites is to prepare graphene with noble metals at a low metal concentration, or graphene with non-noble metals at a high metal concentration. However, recent work shows that nanoplatinum–graphene hybrids with a relatively high metal concentration are competitive, and in some cases demonstrate better performance (Vanegas et al., 2014; McLamore et al., 2011; Shi et al., 2011). Preliminary results indicated that decreasing the ratio of nCe/nPt resulted in reduced performance when detecting superoxide (data not shown). This indicates that molecules which contact the surface of the hybrid nanocomposite have access to both nanoceria and nanoplatinum.

Table 1 summarizes similar carbon/metal nanocomposite-based devices recently reported in the literature in terms of hydrogen peroxide detection (see Kung et al. (2014) for a recent summary of H_2O_2 sensors). The nPt–RGO–nCe-nPt hybrid developed here exhibited an electrochemical performance comparable to most carbon/metal composites in the current literature with a few exceptions. The performance of the nPt–RGO–nCe material is significantly improved over the probe developed by Mehta et al. (2007) using only nCe. The electroactive surface area and sensitivity reported by Shi et al. (2011) are similar to the values reported here. Ensafi et al. (2013) synthesized a hybrid nanocomposite containing exfoliated graphene oxide (EGO) and an antiferromagnetic-metallic oxide (Co_3O_4) on a glassy carbon electrode. The electroactive surface area of the nanocomposite ($\approx 0.134\ cm^2$) and sensitivity ($74.88\ \mu A\ mM^{-1}$) were higher

Table 1
Summary of performance for recent H_2O_2 sensors using similar nanocomposites.

Nanocomposite	Electroactive surface area [$cm^2 \times 10^2$]	Sensitivity [μA/mM]	LOD [μM]	Reference
nPt/RGO/nCe/nPt	6.2 ± 1.5	11.1 ± 3.8	0.5 ± 0.3	This work
mesoporous Pt	NR	$2.8 \pm$ NR	$4.5 \pm$ NR	Evans et al. (2002)
SWCNT/AgNP	$2.0 \pm$ NR	$3.2 \pm$ NR	$0.2 \pm$ NR	Habibi et al. (2012)
nCe	NR	0.48 ± 1.5	$1.0 \pm$ NR	Mehta et al. (2007)
CNT/TMOS	6.2 ± 0.2	12.8 ± 1.9	$3.7 \pm$ NR	Shi et al. (2011)
CNT/GA	5.1 ± 0.7	13.7 ± 2.6	$1.9 \pm$ NR	Shi et al. (2011)
GO/Pt-black	0.6 ± 0.1	4.8 ± 2.2	$1.0 \pm$ NR	Shi et al. (2012)
Graphene/MWCNTs	NR	$0.4 \pm$ NR	$9.4 \pm$ NR	Woo et al. (2012)

NR=value not reported in manuscript.

than the hybrid nanocomposite presented here. From the data presented by Ensafi et al. (2013) it is unclear whether the Co_3O_4 or the EGO was the source of the increased sensitivity toward H_2O_2, and no standard deviation was reported; rendering a direct comparison impossible. Han et al. (2013) describe a hybrid nanomaterial composed of cobalt hexacyanoferrate nanoparticles (CoNP), carbon nanotubes (CNT), and nPt that showed one of the highest known sensitivities toward H_2O_2 (744 μA mM^{-1}). The authors attributed the extremely high sensitivity of this composite to the presence of nPt, which triggered a synergistic electrocatalytic effect when conjugated with CoNPs and CNT. However, CoNPs have demonstrated intrinsic cytotoxicity (Alarifi et al., 2013; Jiang et al., 2012), which limits application in life sciences research and may even render biological elements (such as enzymes) inactive. Dey and Raj (2010) developed a nPt–RGO electrode for detecting H_2O_2 (or cholesterol) at a working potential of +400 mV; the sensitivity toward H_2O_2 was 8.1 μA mM^{-1}, which is lower than the value reported here. The LOD reported by Dey and Raj (2010) (5 nM) was one of the lowest reported detection limits and was significantly lower than the value reported here. However, the working potential of the hybrid material here is 100 mV lower than that of the work by Dey and Raj (2010).

To further test the material developed in this work for use in biosensing, two different enyzmes were immobilized on the nPt–RGO–nCe-nPt hybrid composite. One enzyme (xanthine oxidase) is a hydrophobic enzyme that oxidizes purines and produces superoxide anion (O_2^-). The other enzyme (glucose oxidase) is a hydrophilic enzyme that oxidizes the monosaccharide glucose and produces H_2O_2.

3.2. Nanoceria–platinum–graphene hybrid composite for biosensing

Fig. 4a shows a representative DCPA time series during stepwise injection of glucose for GOx biosensors developed using the hybrid nanocomposite. The average sensitivity for GOx biosensors was 66.2 ± 2.6 μA mM^{-1} cm^{-2} (inset in Fig. 4a). The limit of detection and response time for GOx biosensors using the hybrid nanocomposite was 1.3 ± 0.6 μM, and 6.3 ± 3.4 s, respectively. The coefficient of variation (an index of reliability) for GOx biosensors was 3.9%, which is significantly lower than the values reported from our previous work based on carbon nanotube-nPt hybrid composites (McLamore et al., 2011). GOx produces H_2O_2 as a byproduct from the oxidation of target substrate. The high sensitivity for the GOx is due to electrocatalysis of H_2O_2 by graphene–platinum nanocomposites adjacent to GOx as discussed by Chen et al. (2012) and others.

The average sensitivity (1164 ± 332 μA mM^{-1} cm^{-2}) for xanthine biosensors (Fig. 4b) was much higher than most values previously reported in the literature for carbon/metal-mediated XOD biosensors. The response time (5.0 ± 1.5 s) and limit of detection (0.2 ± 0.1 μM) are lower than other published values (see Table 2). As shown by other researchers (Villalonga et al., 2012) XOD biosensors have no specificity toward xanthine or hypoxanthine. To further challenge XOD biosensors against possible interferences, selectivity was tested in the presence of urea (a known byproduct of purine metabolism); urea caused an interference of 2.3 ± 0.9% in XOD biosensors (see Fig S2a). The coefficient of variation (an index of reliability) for XOD biosensors was 2.8%, which indicates the hybrid nanomaterial is highly reproducible. The unique aspect of XOD biosensors that differentiates them from GOx biosensors is formation of the superoxide anion (O_2^-) as a byproduct of xanthine oxidation. The enhanced performance observed here is due to the synergistic action of nanoceria, which is known to catalyze superoxide dismutation, and subsequent enhancement of H_2O_2 detection by the graphene–platinum nanohybrid. This is a critical advancement in XOD biosensors, as to date no xanthine biosensors have incorporated nanostructures which directly act on O_2^-.

Table 2 shows a comparison of the nCe–RGO–nPt nanocomposite to other biosensors in the literature for glucose or xanthine. Where possible, recipes containing nanoceria or other similar graphene–metal nanocomposites are shown. Most excellent glucose biosensors have a normalized sensitivity in the 20–30 μA $mM^{-1}cm^{-2}$ range (see review by Rahman et al., 2010). The hybrid nanomaterial developed here showed a sensitivity that was over 100 times higher than the nanoceria-GOx biosensor developed by Saha et al. (2009), with a limit of detection approximately 1000 times lower and no need for addition of a mediator. Wu et al. (2012) developed a nanocomposite containing Prussian Blue nanoparticles and the topological insulator bismuth selenide (Bi_2Se_3) with a sensitivity of 24.6 μA mM^{-1} cm^{-2}. While the Bi_2Se_3 nanocomposites are highly suitable for *ex situ* testing, the toxicity of Bi_2Se_3 does not allow development of devices that can be used for physiological studies.

Only Villalonga et al. (2012) reported a carbon/metal-mediated XOD biosensor which displayed performance that was better than the nCe/nPt/RGO hybrid biosensor. The hybrid material by Villalonga et al. (2012) was composed of single-walled carbon nanotubes and a three-dimensional network of electropolymerized gold nanoparticles capped with 2-mercaptoethanesulfonic acid, p-aminothiophenol, and 1-adamantanethiol. However, the authors themselves noted that the sensitivity of their biosensor was significantly influenced by the cyclodextrine (CD) modification to the enzyme (XOD-CD); the same biosensor design without the CD modification resulted in relatively poor analytical performance with shorter linear range, higher LOD, and lower sensitivity. These results suggested that the native enzyme was deficiently loaded in the electrode in comparison with the CD-modified enzyme.

To date, there are only a few other papers which immobilized proteins on CeO_2 nanocomposites for biosensing. Antibodies were immobilized on platinum–CeO_2 nanospheres for development of immunosassays targeting low-abundance proteins; no graphene was utilized in this design (Tang et al., 2013). Antibodies specific to

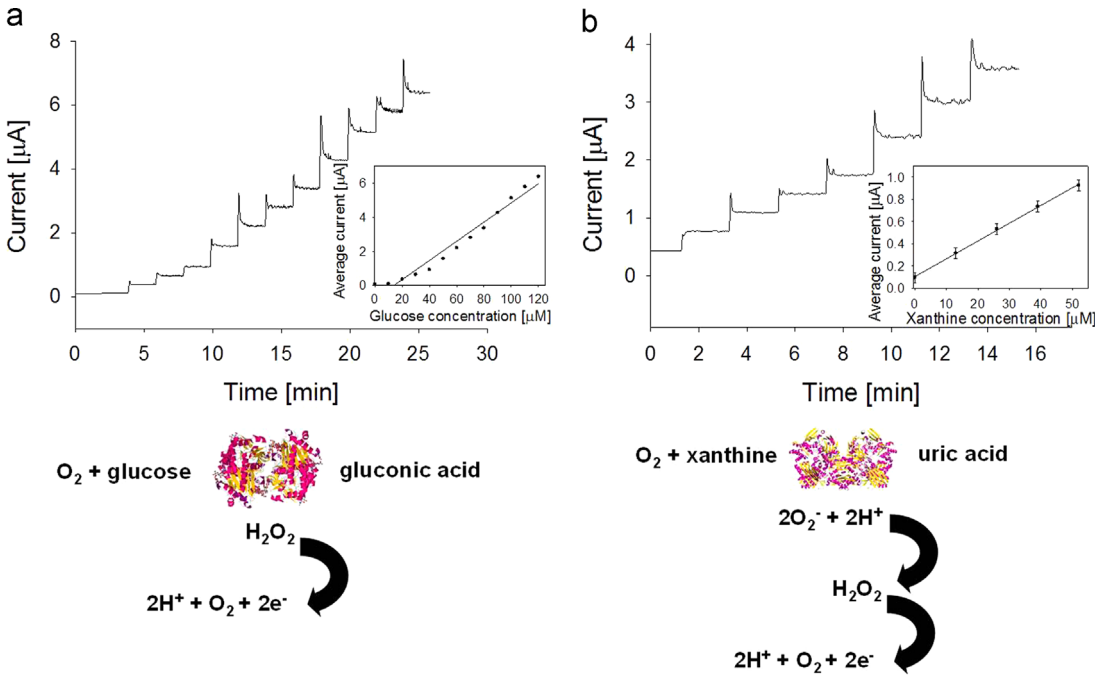

Fig. 4. Sensitivity of glucose and xanthine biosensors based on the nanoceria–graphene–nanoplatinum hybrid nanocomposite. DCPA time series plots and steady state calibration plots of step changes are shown (a) glucose oxidase; a hydrophilic, polar enzyme that oxidizes the monosaccharide glucose to H_2O_2 and (b) xanthine oxidase; a polar, hydrophobic enzyme that oxidizes the purine xanthine to O_2.

Table 2
Performance of amperometric glucose and xanthine biosensors using carbon–metal hybrid nanocomposites.

Biosensor design	Sensitivity [μA mM^{-1} cm^{-2}]	t_{95} [s]	LOD [μM]	Reference
Glucose				
nPt–RGO–nCe–GOx	66.2 ± 2.6	6.3 ± 3.4	1.3 ± 0.6	this work
nCe–nPt	0.5 ± 0.1	NR	1300.0 ± NR	Saha et al. (2009)
TEOS/GOx	1.2 ± 0.1	< 8.0	2.0 ± NR	Shi et al. (2011)
MWNT/Nafion/ Ox/GCE	0.3 ± NR	< 8.0	4.0 ± NR	Shi et al. (2011)
Au/MWNT/GOx	1.7 ± NR	< 16.0	10.0 ± NR	Wang et al., (2003)
SWNT/nPt/GOx	2.1 ± NR	3.0 ± NR	0.5 ± NR	Hrapovic et al., (2004)
Xanthine				
nPt–RGO–nCe–XOD	1164 ± 332	5 ± 1.5	0.2 ± 0.1	this work
XOD/ZnO–NP/CHIT/MWCNT/PANI	NR	4.0 ± NR	0.1 ± NR	Devi et al., (2012)
XOD–AuNP–SWCNH	141.1 ± NR	NR	0.7 ± NR	Zhang et al., (2012)
XOD/SnO_2 QD/ITO	514.8	10.0 ± NR	1.0 ± NR	Kamil-Reza et al. (2013)

NR = not reported.

carcinoembryonic antigen (CEA) were conjugated to Pt–CeO_2 nanocomposites and immobilized on a glassy carbon electrode. The approach combined redox cycling with an in situ signal amplification strategy for determining CEA concentration. The other approach by Zhang et al. (2013) immobilized cholesterol oxidase on a CeO_2–graphene nanocomposite for measuring cholesterol (Zhang et al., 2013). Although this approach involved cholesterol oxidase, the authors did not monitor oxidative current from the oxidase enzyme (the most common method in the literature). Instead, an optical approach was used to monitor oxidation of cholesterol via luminol fluorescence. Ansari et al. (2008) and Anees et al. (2008) demonstrated cholesterol and glucose biosensors using nanoceria, but no carbon materials were used as a transduction layer. Panky et al. (2013) developed nanostructured CeO_2 thin films together with cadmium oxide for butyrin sensing using lipase as the biorecognition element. To date, no papers have investigated the use of nCe–RGO–nPt as a transducing film in biosensing.

While the nanocomposite here demonstrated remarkable performance and is a promising platform for biosensing, precise control over the CeO_2 valence (and therefore oxygen vacancies) was not possible. Utilizing graph from (i.e., bottom-up) synthesis approaches such as those by Jiang et al. (2012), and Joung et al. (2011) would likely improve control of the nanocomposites for biosensor applications. However, the simple, room temperature approach here represents a significant improvement in the performance of oxidase-based biosensors. Studies have shown that CeO_2 nanoparticles are non-toxic in mammalian cells, and may even be beneficial for ROS scavenging (Xia et al., 2008). Although toxicity of the hybrid nanocomposite developed here is unknown, the biocompatibility of the individual nanoparticles (nCe, nPt, and RGO) indicates that next generation implantable devices may be able to utilize the catalytic platform developed here for in vivo biosensing applications.

4. Conclusion

Within the field of biosensing, oxidase enzymes that produce hydrogen peroxide are one of the most prominent recognition agents, and superoxide-producing enzymes are emerging as

prominent enzymes for biosensing. This paper is the first effort reporting on the combined effects of nanoplatinum, nanoceria, and graphene as a transducer layer between proteins and metal electrodes. The hybrid nanocomposite developed here demonstrated highly efficient electron transport as a base transducing layer for mediator-free enzymatic biosensors. In enzymatic biosensing, the combination of nanoceria with nanoplatinum-decorated graphene provides an important advantage: selective catalysis of superoxide (by nanoceria) or hydrogen peroxide (by platinum–graphene). When comparing nCe/nPt/RGO biosensors to other devices that have been used for minimally invasive glucose biosensing, the sensitivity, response time, and limit of detection are within the same range as previously reported values; sensitivity and limt of detection were orders of magnitude better than previously reported glucose biosensors using only nCe as the transducer platform. Remarkably, XOD biosensor sensitivity, response time, and limit of detection were higher than any reported biosensors using similar metal-decorated carbon nanomaterials.

Acknowledgments

The authors would like to thank the Colombian funding agency COLCIENCIAS, the Agricultural and Biological Engineering Department of the University of Florida, and the UF Early Career Award for their support. We also thank PIKL (Baltimore, MD) for their help with graphic images.

Appendix A. Supporting information

Supplementary data associated with this article can be found in the online version at http://dx.doi.org/10.1016/j.bios.2014.02.021.

References

Adachi, G.Y., Imanaka, N., 1997. J. Alloys Compd. 250, 492–500.
Akhavan, O., 2011. Carbon 49, 11–18.
Alarifi, S, Verma, A., Alakhtani, S., Ali, B.A., 2013. J. Toxicol. 32, 296–307.
Anees, A., Kaushik, A., Solanki, P.R., Malhotra, B.D., 2008. Electrochem. Commun. 10, 1246–1249.
Ansari, A.A., Solanki, P.R., Malhotra, B.D., 2008. Appl. Phys. Lett 92, 263901–263903.
Aravind, S.S.J., Eswaraiaha, V., Ramaprabhu, S., 2011. J. Mater. Chem. 21, 17094–17097.
Asati, A., Santra, S., Kaittanis, C., Nath, S., Perez, J.M., 2009. Angew. Chem. 48, 2308–2312.
Bai, S., Shen, X., 2012. RSC Adv. 2, 64–98.
Bolotin, K.I., Sikes, K.J., Jiang, Z., Klima, M., Fudenberg, G., Hone, J., 2008. Solid State Commun. 146, 351–355.
Chen, L., Wang, X., Zhang, X., Zhang, H., 2012. J. Mater. Chem. 22, 22090–22096.
Claussen, J.C., Artiles, M.S., McLamore, E.S., Mohanty, S., Shi, J., Rickus, J.L., Fisher, T.S., Porterfield, D.M., 2011. J. Mater. Chem. 21, 11224–11231.
Devi, R., Yadav, S., Pundir, C.S., 2012. Analyst 137, 754–759.
Dey, R.S., Raj, C.R., 2010. J. Phys. Chem. C 114, 21427–21433.
Du, J., Lai, X.Y., Yang, N.L., Zhai, J., Kisailus, D., Su, F.B., Wang, D., Jiang, L., 2011. ACS Nano 5, 590–596.
Dua, V., Surwade, S.P., Ammu, S., Agnihotra, S.R., Jain, S., Roberts, K.E., Park, S., Ruoff, R.S., Manohar, S.K., 2010. Angew. Chem. Int. Ed. 122, 2200–2203.
Ensafi, A., Jafari-Asl, M., Rezaei, B., 2013. Talanta 103, 322–329.
Evans, S.A.G., Elliott, J.M., Andrews, L.M., Bartlett, P.N., Doyle, P.J., Denuault, G., 2002. Anal. Chem. 74, 1322–1326.
Gaynor, J.D., Karakoti, A.S., Inerbaev, T., Sanghavi, S., Nachimuthu, P., Shutthanandan, V., Seal, S., Thevuthasan, S., 2013. J. Mater. Chem. B 1, 3443–3450.
Geim, A.K., 2009. Science 6, 1530–1534.
Geim, A.K., Novoselov, K.S., 2007. Nat. Mater. 6, 183–191.
Habibi, B., Jahanbakhshi, M., Pournaghi-Azar, M., 2012. Microchim. Acta 177, 185–193.
Han, L., Wang, Q., Tricard, S., Liu, J., Fang, J., Zhao, J., Shen, W., 2013. RSC Adv. 3, 281–287.
Hrapovic, S., Liu, Y., Male, K.B., Luong, J.H., 2004. Anal. Chem. 76, 1083–1088.
Huang, X., Qi, X.Y., Boey, F., Zhang, H., 2012. Chem. Soc. Rev. 41, 666 (86).
Huang, L., Pan, Y., Pan, L., Gao, M., Xu, W., Que, Y., Zhou, H., Wang, Y., Du, S., Gao, H.J., 2011. Appl. Phys. Lett. 99, 163107.
Ji, Z., Shen, X., Li, M., Zhou, H., Zhu, G., Chen, K., 2013. Nanotechnology 24, 115603–115612.
Jiang, L., Yao, M., Liu, B., Li, Q., Liu, R., Lv, H., Lu, S., Gong, C., Zou, B., Cui, T., Liu, B., 2012. J. Phys. Chem. C 116, 11741–11745.
Jiang, L., Yao, M., Liu, B., Li, Q., Liu, R., Yao, Z., Lu, S., Cui, W., Hua, X., Zou, B., Cui, T., Liu, B., 2013. Cryst Eng Comm 15, 3739–3743.
Joung, D., Singh, V., Park, S., Schulte, A., Seal, S., Khondaker, S.I., 2011. J. Phys. Chem. C 115, 24494–24500.
Kamil-Reza, K., Singh, M.K., Yadav, S.K., Singh, J., Agrawal, V.V., Malhotra, B.D., 2013. Sens. Actuators B: Chem. 177, 627–633.
Kim, K.S., Zhao, Y., Jang, H., Lee, S.Y., Kim, J.M., Kim, K.S., Ahn, J.H., Kim, P., Choi, J.Y., Hong, B.H., 2009. Nature 457, 706–710.
Kung, C.C., Lin, P.Y., Buse, F.J., Xue, Y., Yu, X., Dai, L., Liu, C.C., 2014. Biosens. Bioelectron. 52, 1–7.
Li, N., Cao, M.H., Hu, C.W., 2012. Nanoscale 4, 6205–6218.
Li, D., Muller, M.B., Gilje, S., Kaner, R.B., Wallace, G.G., 2008. Nat. Nanotechnol. 3, 101–105.
Liang, Y.Y., Li, Y.G., Wang, H.L., Zhou, J.G., Wang, J., Regier, T., 2011. Nat. Mater. 10, 780–786.
Lu, X.H., Zhai, T., Cui, H.N., Shi, J.Y., Xie, S.L., Huang, Y.Y., Liang, C.L., Tong, Y.X., 2011. J. Mater. Chem. 21, 5569–5572.
Luo, B., Wang, B., Liang, M.J., Ning, J., Li, X.L., Zhi, L.J., 2012. Adv. Mater. 24, 1405–1409.
McLamore, E.S., Shi, J., Jaroch, D., Claussen, J.C., Uchida, A., Jiang, Y., Zhang, W., Donkin, S.S., Banks, M.K., Buhman, K.K., Teegarden, D., Rickus, J.L., Porterfield, D. M., 2011. Biosens. Bioelectron. 26, 2237–2245.
Mehta, A., Patel, S., Bang, H., Cho, H.J., Seal, S., 2007. Sens. Actuat. B Chem., 146–151
Neil, J.L., Joseph, R.B., Wang, L., Wu, T.S., Jamie, W.K., Marcella, M.I., Wang, G.H., Soo, Y.L., Mei, W.L., Cheung, W.L, 2011. Nano Lett. 11, 2666–2671.
Nyk, M., Kumar, R., Ohulchanskyy, T.Y., Bergey, E.J., Prasad, P.N., 2008. Nano Lett. 8, 3834–3838.
Panky, S., Thandavan, K., Sivalingam, D., Sethuraman, S., Maheswari, U., Jeyaprakash, K.B.G., Rayappan, J.B.B., 2013. Mater. Chem. Phys. 137, 892–897.
Rahman, M.M., Ahammad, J.S., Jin, J.-H., Ahn, S.J., Lee, J.-J., 2010. Sensors 10, 4855–4886.
Rao, C.N.R., Sood, A.K., Subrahmanyamand, K.S., Govindaraj, A., 2009. Angew. Chem. Int. Ed. 48, 7752–7777.
Saha, S., Arya, S.K., Singh, S.P., Sreenivas, K., Malhotra, B.D., Gupta, V., 2009. Biosens. Bioelectron. 24, 2040–2045.
Schniepp, H.C., Li, J.L., McAllister, M.J., Sai, H., Herrera-Alonso, M., Adamson, D.H., Prud'homme, R.K., Car, R., Saville, D.A., Aksay, I.A., 2006. J. Phys. Chem. B. 110, 8535–8539.
Shi, J., Claussen, J.C., McLamore, E.S., ul Haque, A., Jaroch, D., Diggs, A.R., Calvo-Marzal, P., Rickus, J.L., Porterfield, D.M., 2011. Nanotechnology 22, 1–10.
Shi, J., Zhang, H., Snyder, A., Wang, M., Xie, J., Porterfield, D.M., Stanciu, L.A., 2012. Biosens. Bioelectron. 38, 314–320.
Solanki, P.R., Dhand, C., Kaushik, A., Ansari, A.A., Soud, K.N., Malhotra, B.D., 2009. Sens. Actuat. B: Chem, 551–556.
Stankovich, S., Dikin, D.A., Piner, R.D., Kohlhaas, K.A., Kleinhammes, A., Jia, Y., Wu, Y., Nguyen, S.T., Ruoff, R.S., 2007. Carbon 45, 1558–1565.
Stankovich, S., Dikin, D.A., Dommett, G.H.B., Kohlhaas, K.M., Zimney, E.J., Stach, E.A., Piner, R.D., Nguyen, S.T., Ruoff, R.S., 2006. Nature 442, 282–286.
Sun, X., Wang, Y., Li, D.Y., 2013. Wear 301, 406–414.
Tang, J., Zhou, J., Li, Q., Tang, D., Chen, G., Yang, H., 2013. Chem. Commun. 49, 1530–1532.
Vanegas, D.C., Taguchi, M., Chaturvedi, P., Burrs, S.L., Tan, M., Yamaguchi, H., McLamore, E.S., 2014. Analyst 39, 660–667.
Villalonga, R., Díez, P., Eguílaz, M., Martínez, P., Pingarrón, J.M., 2012. ACS Appl. Mater. Interf. 4, 4312–4319.
Wang, G.X., Yang, J., Park, J., Gou, X.L., Wang, B., Liu, H., Yao, J., 2008. J. Phys. Chem. C. 112, 8192–8195.
Wang, S.G., Zhang, Q., Wang, R., Yoon, S.F., Ahn, J., Yang, D.J., Tian, J.Z., Li, J.Q., Zhou, Q., 2003. Electrochem. Commun. 5, 800–803.
Wang, D.W., Li, F., Zhao, J.P., Ren, W.C., Chen, Z.G., Tan, J., Wu, Z.S., Gentle, I., Lu, G.Q., Cheng, H.M., 2009. ACS Nano 7, 1748–1752.
Wang, G., Bai, J., Wang, Y., Ren, Z., Bai, J., 2011. Scr. Mater. 65, 339–342.
Woo, S., Kim, Y.R., Chung, T.D., Piao, Y., Kim, H., 2012. Electrochim. Acta 59, 509–514.
Wu, S., Liu, G., Li, P., Liu, H., Xu, H., 2012. Biosens. Bioelectron. 38, 289–294.
Wu, Z.S., Ren, W.C., Wang, D.W., Li, F., Liu, B.L., Cheng, H.M., 2010a. ACS Nano 10, 5835–5842.
Wu, Z.S., Wang, D.W., Ren, W.C., Zhao, J.P., Zhou, G.M., Li, F., Cheng, H.M., 2010b. Adv. Funct. Mater. 20, 3595–3602.
Wu, L., Zhang, X., Ju, H., 2007. Biosens. Bioelectron. 23, 479–484.
Xia, T., Kovochich, M., Liong, M., Madler, L., Gilbert, B., Shi, H., Yeh, J.I., Zink, J.I., Nel, A.E., 2008. ACS Nano 10, 2121–2134.
Yang, J., Heo, M., Lee, H.J., Park, S.M., Kim, J.Y., Shin, H.S., 2011. ACS Nano 10, 8365–8371.
Zhang, F., Braun, G.B., Shi, Y.F., Zhang, Y.C., Sun, X.H., Reich, N.O., Zhao, D.Y., Stucky, G., 2010a. J. Am. Chem. Soc. 132, 2850–2851.
Zhang, F., Deng, Y.H., Shi, Y.F., Zhang, R.Y., Zhao, D.Y., 2010b. J. Mater. Chem. 20, 3895–3900.
Zhang, H., Lv, X.J., Li, Y.M., Wang, Y., Li, J.H., 2010c. ACS Nano 2010 (1), 380–386.
Zhang, L., Lei, J., Zhang, J., Ding, L., Ju, H., 2012. Analyst 137, 3126–3131.
Zhang, M., Yuan, R., Chai, Y., Wang, C., Wu, X., 2013. Anal. Biochem. 436, 69–74.
Zhou, K., Wang, X., Sun, X., Peng, Q., Li, Y., 2005. J. Catal. 229, 206–212.
Zhu, Y., Murali, S., Cai, W., Li, X., Suk, J.W., Potts, J.R., Ruoff, R.S., 2010. Adv. Mater. 22, 3906–3924.